Surface Science 624 (2014) 145–153

Contents lists available at ScienceDirect

Surface Science

journal homepage: www.elsevier.com/locate/susc

The growth of cobalt oxides on HOPG and SiO_2 surfaces: A comparative study

D. Díaz-Fernández [a], J. Méndez [b], O. Bomatí-Miguel [a], F. Yubero [c], R.J.O. Mossanek [d], M. Abbate [d], G. Domínguez-Cañizares [a], A. Gutiérrez [a], S. Tougaard [e], L. Soriano [a,*]

[a] Departamento de Física Aplicada and Instituto de Ciencia de Materiales Nicolás Cabrera, Universidad Autónoma de Madrid, Cantoblanco, E-28049 Madrid, Spain
[b] Grupo ESISNA, Instituto de Ciencia de Materiales de Madrid, ICMM-CSIC, Cantoblanco, E-28049 Madrid, Spain
[c] Instituto de Ciencia de Materiales de Sevilla, (ICMSE-CSIC-US), Avda. AmericoVespuccio 49, Isla de la Cartuja, E-41092 Sevilla, Spain
[d] Departamento de Física, Universidade Federal do Paraná, Caixa Postal 19044, 81531-990 Curitiba, PR, Brazil
[e] Department of Physics, Chemistry and Pharmacy, University of Southern Denmark, DK-5230 Odense M, Denmark

ARTICLE INFO

Article history:
Received 16 November 2013
Accepted 4 February 2014
Available online 16 February 2014

Keywords:
Co oxides
Oxide growth
XPS
AFM

ABSTRACT

The growth of cobalt oxides by reactive thermal evaporation of metallic cobalt on highly oriented pyrolytic graphite (HOPG) and SiO_2 (X cut quartz surface), in an oxygen atmosphere at room temperature, has been chemically and morphologically studied by means of X-ray photoelectron spectroscopy and atomic force microscopy. The chemical analysis, which also includes cluster calculations, reveals that for the early deposition stages on both substrates, Co^{2+} species are stabilized at the surface up to a coverage which depends on the substrate. Further coverages lead to the formation of the spinel oxide Co_3O_4. The results are discussed in terms of the dependence of the surface energy on the size of the CoO deposited moieties. On the other hand, it has been found that the initial way of growth of cobalt oxides on HOPG is of Stranski–Krastanov mode whereas on SiO_2 the growth is of Volmer–Weber mode. The differences in the growth morphology have been discussed in terms of the surface diffusivity of the CoO deposits on the substrates.

1. Introduction

The main purpose of this paper is to study the growth of cobalt oxide thin films on two substrates with different electronic structures, an inert and conductive surface, such as highly oriented pyrolytic graphite (HOPG) and a reactive and insulating surface such as SiO_2 single crystal. It is known that the growth mechanism of a thin film of any material can be strongly affected by the chemical nature and morphology of the support. The interaction of the surface atoms of the substrate with the adsorbates can be affected by many effects such as surface diffusion, aggregation, surface and interface chemical reactivity, and desorption which can play an important role in the final properties of the film [1–3]. These effects are particularly important at the early stages of the film growth, where the growing material is in direct contact with the support.

To study the cobalt oxide thin film growth mechanisms, we have used two complementary characterization techniques: atomic force microscopy (AFM) and X-ray photoemission spectroscopy (XPS). Whereas AFM is a local direct probe of the topography of the sample surface at the nanometer scale, XPS provides information on the surface chemistry. The XPS chemical analysis is supported by theoretical cluster model calculations of the photoelectron spectra for the different Co oxide species. In addition, using inelastic XPS peak shape analysis given by the Tougaard algorithms [4], implemented in the QUASES software [5], the averaged in-depth distribution of the elements at the topmost surface layers of a sample can be obtained. We show below that with the combination of these two techniques, a detailed description of the way of growth of Co oxides on those very different substrates can be obtained.

The family of cobalt oxides is reduced to two stable oxides at room temperature: CoO (Co^{2+}), which grows with a halite structure (a = 4.260 Å) [6] and Co_3O_4 ($Co^{2+,3+}$), which is characterized by a spinel structure (a = 8.084 Å) [7]. Also the existence of cobaltic oxide Co_2O_3 (Co^{3+}) with a corundum structure (a = 4.882 Å, c = 13.38 Å) has been reported, but it is metastable, appearing always in combination with other cobalt oxides or other compounds [8]. CoO and Co_3O_4 have recently attracted a great interest in materials research due to their applications as super-capacitors [9–11] and the improvements they provide to traditional applications such as anodes on lithium-ion batteries [12], catalyst in water oxidation reactions [13] and oxygen reduction reactions when supported on graphene [14], gas sensors [15,16] and magnetoresistant [17] and electrochromic [18,19] materials.

The study of oxide/oxide interfaces has recently become a hot topic mainly due to their unique properties such as interface

* Corresponding author.
E-mail address: l.soriano@uam.es (L. Soriano).

http://dx.doi.org/10.1016/j.susc.2014.02.007
0039-6028/

Table 1
Cluster model parameters (all values in eV).

Parameter	Co^{2+}	Co^{3+}
Δ	5.5	4.0
U	5.2	5.0
pdσ	1.3	1.9
10 Dq	0.70	1.0
B	0.14	0.15
C	0.54	0.60

superconductivity, magneto-electric coupling and quantum Hall effect in oxide heterostructures [20]. Most of the recent research in the characterization of the early stages of the growth of oxides, including cobalt oxides, has been done on metal surfaces [21–23], however works studying the growth of oxide-oxide interfaces are very scarce. This has been mainly due to the difficulty in their characterization by electron spectroscopies given the insulating character of most of the oxides, which leads to charging effects thus avoiding their efficient characterization. In spite of this, works dealing with oxide/oxide interfaces studied by electron spectroscopies can be found elsewhere [24]. In particular, the growth of cobalt oxides on SiO_2 [25] and Al_2O_3 [26] supports has already been studied. For polycrystalline SiO_2 substrate, CoO (Co^{2+}) species have been found to grow upon oxidation with molecular oxygen gas, whereas Co_3O_4 ($Co^{2+,3+}$) species have been obtained upon oxidation using oxygen plasma. In the case of the alumina substrate, XPS has revealed sudden changes in the shape of the Co 2p lines from 3.4 Å to 17 Å cobalt oxide thicknesses, indicating the transition from an interfacial cobalt oxide (Co^{2+}) layer toward (111) oriented Co_3O_4 [26]. In spite of the importance of Co and CoO as catalysts in the growth of Carbon nanotubes (CNT's) [27], no specific studies dealing with the growth of cobalt oxides on HOPG have been found in the literature. Only one study of oxidized Co particles on HOPG has been reported [28]. The lack of detailed studies on this subject makes the present work more relevant.

Regarding the substrates studied here, HOPG presents a very inert surface with weak π bonds perpendicular to the surface plane and

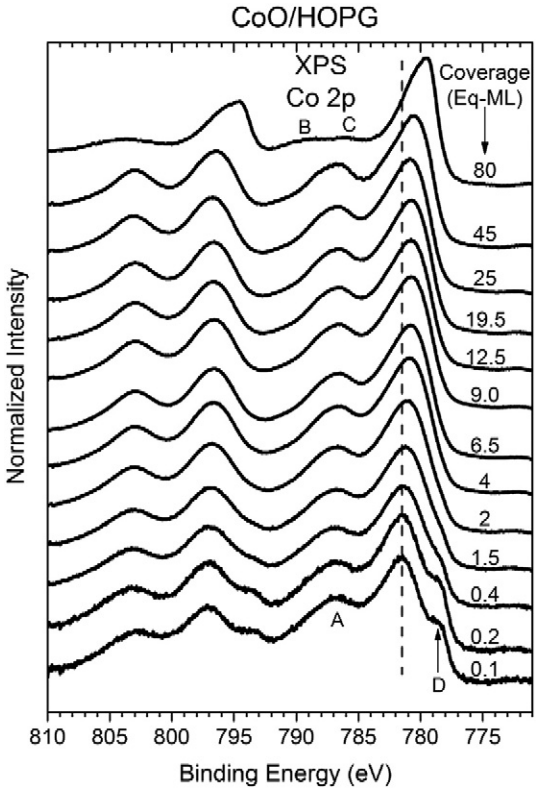

Fig. 1. Co 2p XPS spectra for the growth of Co oxides on HOPG as a function of coverage (as labeled).

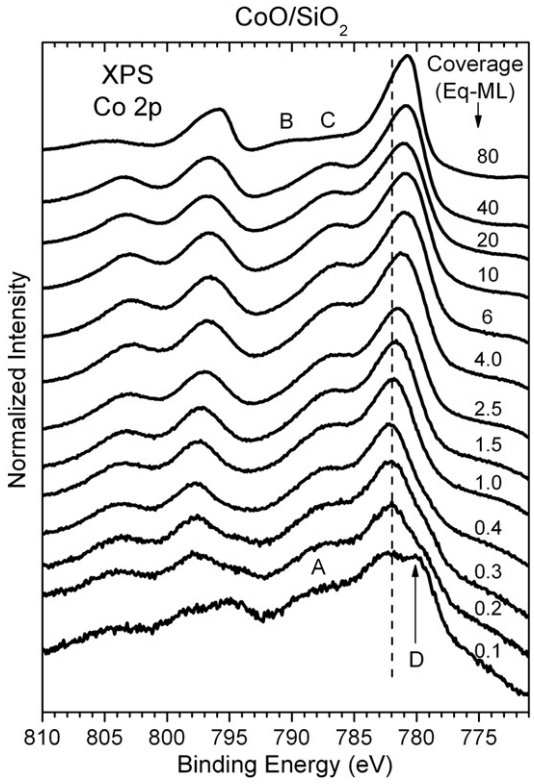

Fig. 2. Co 2p XPS spectra for the growth of Co oxides on SiO_2 as a function of coverage (as labeled).

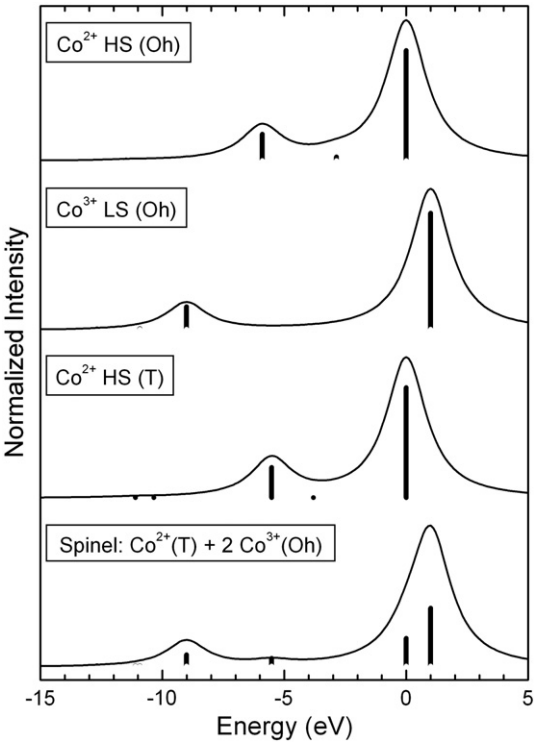

Fig. 3. Cluster model calculations of the Co 2p XPS spectra for different Co ions and symmetries.

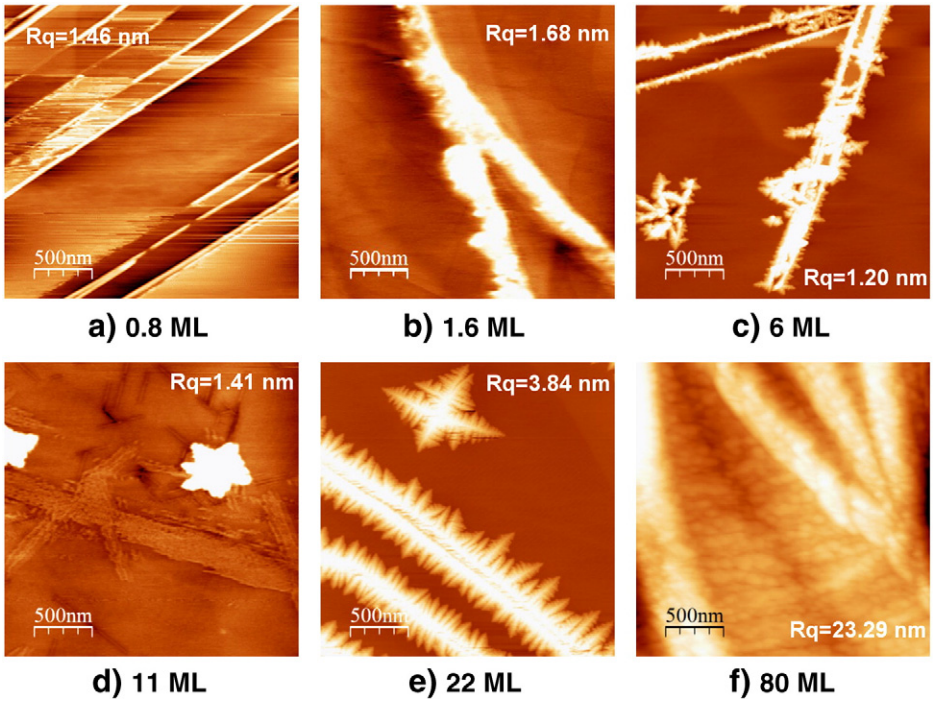

Fig. 4. 2.5 × 2.5 μm^2 AFM images of the growth of Co oxides on HOPG for different coverages. The root mean square roughness (Rq) values are given.

strong σ C–C bonds localized in the surface plane. In contrast, the SiO_2 surface used in this work (X cut quartz) is much more reactive due to its termination in coordinately unsaturated oxygen anion centers [29]. As a consequence of this reactivity, the formation of M–O–Si (M = Metal) cross linking bonds has been observed in the growth of different transition metal oxides on SiO_2 [30–33]. In both cases, we are dealing with flat surfaces with roughness under the nanometer scale.

2. Experimental details and methods

Cobalt oxide was grown by thermal evaporation of metallic cobalt in a molecular oxygen atmosphere ($PO_2 = 2 \times 10^{-5}$ mbar), with 1×10^{-8} mbar as base pressure of the chamber and maintaining the substrates at room temperature. A HOPG substrate from Goodfellow was first cleaved using a scotch tape and then heated at 400 °C under vacuum conditions (3×10^{-8} mbar). The SiO_2 substrate was an X cut quartz single crystal from MTI Corporation with a nominal mean roughness of 3 Å. It was also heated under ultra-high-vacuum conditions (3×10^{-8} mbar, 450 °C) to remove surface contamination. The evaporation rate was maintained constant and very low (≈0.2 Å/min) to allow the study of the very early stages of growth, i.e. coverages below one equivalent monolayer (Eq-ML). The growth process was performed in a preparation chamber attached to the XPS spectrometer. Successive evaporations were performed and after each step the surface was analyzed by XPS.

The XPS measurements were performed with a CLAM-4 MCD hemispherical analyzer system from Thermo Fisher Scientific using a twin-anode source. The measurements were performed at 0° take-off angle (surface plane of the sample perpendicular to the XPS lens spectrometer edge). The spectra of the cobalt oxide deposits on HOPG were measured using the Mg anode whereas those corresponding to the deposits on the silica substrate were measured using the Al anode to avoid overlap of the oxygen Auger peaks with the Co 2p energy region. The pass energy of the analyzer was set to 20 eV, giving a resolution of about 0.9–1.0 eV respectively depending on the anode used, Mg or Al. The energy scale was calibrated by adjusting the Si 2p3/2 XPS peak for SiO_2 at 103.0 eV for the spectra of the silica substrate and the C1s peak at 284.3 eV for those of the HOPG substrate. Ex-situ AFM images were obtained with a Nanotec AFM microscope in non-contact dynamic (tapping) mode, using commercial tips from Nanosensors. The images were processed and analyzed with the WSxM software [34].

Core level spectra of different Co ion configurations were calculated using a standard cluster model [35]. The cluster consists of a Co ion surrounded by oxygen ions in octahedral (CoO_6) or tetragonal (CoO_4) symmetries. The main parameters of this model are the d–d Coulomb interaction U, the charge transfer energy Δ and the p–d hybridization pdσ. The cluster is solved with the configuration interaction scheme [36], where the ground and final states are expanded in configuration of the type $3d^{n+k}\underline{L}^k$, where $\underline{L}$ denotes a hole in the oxygen band. Each configuration is further split into different multiplets, which are given in terms of the Racah parameters *B* and *C* and the crystal field 10 Dq. The parameters used in this calculation are in agreement with previous works [37] and are given in Table 1. The cluster model is then solved with exact diagonalization and the spectral weight is calculated using the sudden approximation.

Both, XPS and AFM can give quantitative information on the growth mechanisms. XPS provides this information in two ways: by integrating the intensity of the core-level peaks and by analyzing the background produced by inelastic electrons. We have performed a quantitative analysis of the XPS intensities following an exponential growth method applied to the Co 2p XPS peak [38]. This allowed us to determine the coverage of the deposited material in equivalent monolayers (Eq-ML's), i.e. the number of equivalent monolayers of the material present on the substrate. According to the dimensions of the CoO unit cell given by Wyckoff [39], we have taken 1 ML as 2 Å thick, i.e. half of the lattice parameter. The XPS spectra and AFM images shown in this work have been labeled using this procedure. On the other hand, the inelastic peak shape analysis [4] for elemental in-depth profiling at the top-most surface region is a non-destructive method based on the quantitative description of the peak shape caused by the inelastic scattering of the emitted photoelectron and Auger peaks in XPS experiments. It has been implemented in the QUASES software [5,40] and is appropriate to study the morphology and the initial growth mechanisms of thin films grown in situ, especially in systems where no probe microscopes are available [41]. It has been applied to a wide range of materials, in particular to the growth of NiO on HOPG [42]

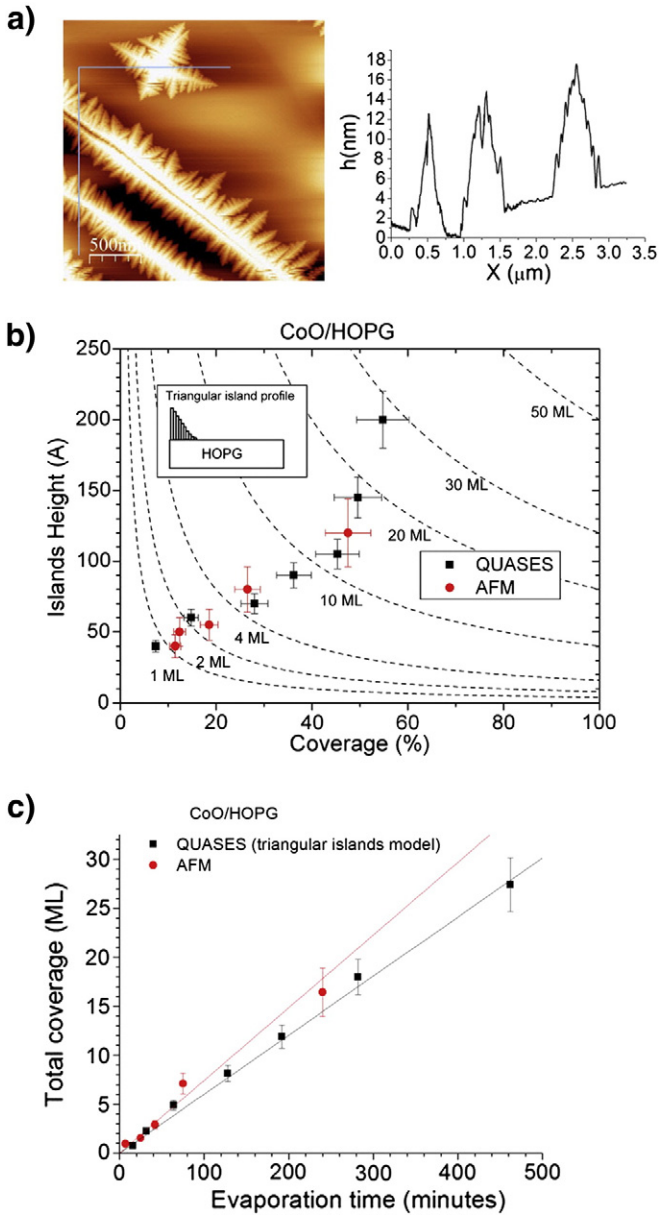

Fig. 5. a) AFM image and topography profile of dendritic islands accumulated at the steps and terraces for a coverage of 22 Eq-ML of CoO on HOPG; b) comparison of the quantitative analysis given by AFM (red dots) and inelastic XPS peak shape analysis using a triangular islands profile (black squares); c) comparison of the total amount of deposited material as a function of the evaporation time given by AFM (red dots) and inelastic XPS peak shape analysis (black squares).

and oxide substrates [30]. The method allows estimating the elemental in-depth profile (surface coverage and island height) of an adsorbate on a substrate. It relies on a trial-and-error procedure where the parameters describing the in-depth profile (average or distribution of island height, surface coverage, etc.) are varied until a satisfactory description of the inelastic peak shape of a photoemitted electron peak is achieved. The method allows estimating the growth mechanism (layer by layer, islands, intermediate, etc.) in the initial stages of thin film growth. AFM gives direct information on the topography of the surface. Although AFM images taken in topography mode can give directly the islands' height and an estimate of the total coverage of the sample by means of flood analysis of the images, it is difficult to quantify the total amount of deposited material, thus a quantitative comparison with other technique such as XPS is important in order to obtain reliable information.

In this work we first present a chemical analysis of the Co species found in the growth process using the experimental XPS spectra and theoretical cluster calculations. Then, by combining both, AFM and inelastic XPS peak shape analysis, we have studied the morphology and way of growth of the cobalt oxides on both substrates. By considering the information obtained from the AFM images (islands' heights, formation of a wetting layer, double layer of islands, etc.), we have used the most suitable in-depth profile model within the inelastic peak shape analysis to obtain the total deposited material as a function of the deposition time. We show below that by forcing the consistency between the AFM and QUASES analysis, a very complete and reliable description of the growth mechanism of the cobalt oxide films on the HOPG and SiO_2 substrates is achieved.

3. Results and discussion

3.1. Chemical analysis

Co 2p XPS spectra of the cobalt oxides deposited on HOPG and SiO_2 as a function of the coverage are shown in Figs. 1 and 2, respectively. All spectra are labeled with their corresponding equivalent coverage. In general, the spectra shown in Fig. 1 have a similar lineshape except for the spectra corresponding to very low coverages (<1 Eq-ML) and the spectra for large coverage (80 Eq-ML). The Co $2p_{3/2}$ region of the spectra consists of a main peak located at a binding energy of 782.0 eV and a satellite (labeled A in Fig. 1) at 788.0 eV. However, for coverages below 1 Eq-ML, a new small shoulder at a binding energy close to 779.0 eV, labeled D in Fig. 1, appears. This shoulder is assigned to some metallic Co which still remains unoxidized, in agreement with other published data [43]. On the other hand, the spectrum for high coverages (80 Eq-ML) shows the main line at a binding energy of c.a. 780.0 eV and the splitting of the satellite A into two weak peaks (labeled B and C in Fig. 1). The Co $2p_{3/2}$ XPS spectra for different stages of the growth of cobalt oxide on SiO_2 are depicted in Fig. 2. These spectra show the same shape and behavior as for the HOPG substrate. The presence of metallic cobalt (feature D) in the case of low coverages and the splitting of feature A into B and C peaks for large coverages (80 Eq-ML), are also observed.

In order to identify the observed chemical species present during the growth process, we have used cluster model calculations to obtain the theoretical Co $2p_{3/2}$ XPS spectra for different Co species. The results are presented in Fig. 3, where the relative energy positions of the different final states are related to the position of the main peak in the top spectrum (Co^{2+} HS Oh). The top spectrum (i.e. for the case of Co^{2+} ($3d^7$)) ions in high spin configuration and octahedral symmetry (HS Oh), consist of a main peak and a charge transfer satellite separated by about 6.0 eV. The spectrum labeled Co^{3+} LS (Oh) is for the case of Co^{3+} ($3d^6$) ions in low spin configuration and octahedral symmetry (LS Oh). Here, the main peak is chemically shifted by around 1.0 eV, in comparison to the previous spectrum, and the splitting between the main peak and the satellite is now about 10 eV. Finally, the spectrum labeled Co^{2+} HS (T) is for the case of Co^{2+} ($3d^7$) ions in high spin configuration and tetragonal symmetry (HS T). Here the spectrum is very similar to the octahedral one, but the separation between main peak and satellite is reduced to around 5.5 eV, due to the reduced effective hybridization. The lowest spectrum labeled Co^{2+} (T) + 2 Co^{3+} (Oh) is calculated to account for a spinel structure, which is possible in cobalt oxides. This is done by using a combination of the spectra for one Co^{2+} (HS T) and two of Co^{3+} (LS Oh).

Comparing these calculated spectra to the experimental spectra in Figs. 1 and 2, it is clear that the main peak and the satellite peak shifted by 6 eV observed for low coverages correspond to the peaks in the upper spectrum of Fig. 3. We can therefore conclude that low coverage cobalt oxide grows as CoO (Co^{2+} in high spin configuration and in octahedral symmetry) on both substrates. This result agrees with those of Ref [25]. For the HOPG substrate the spectra are dominated by CoO species for

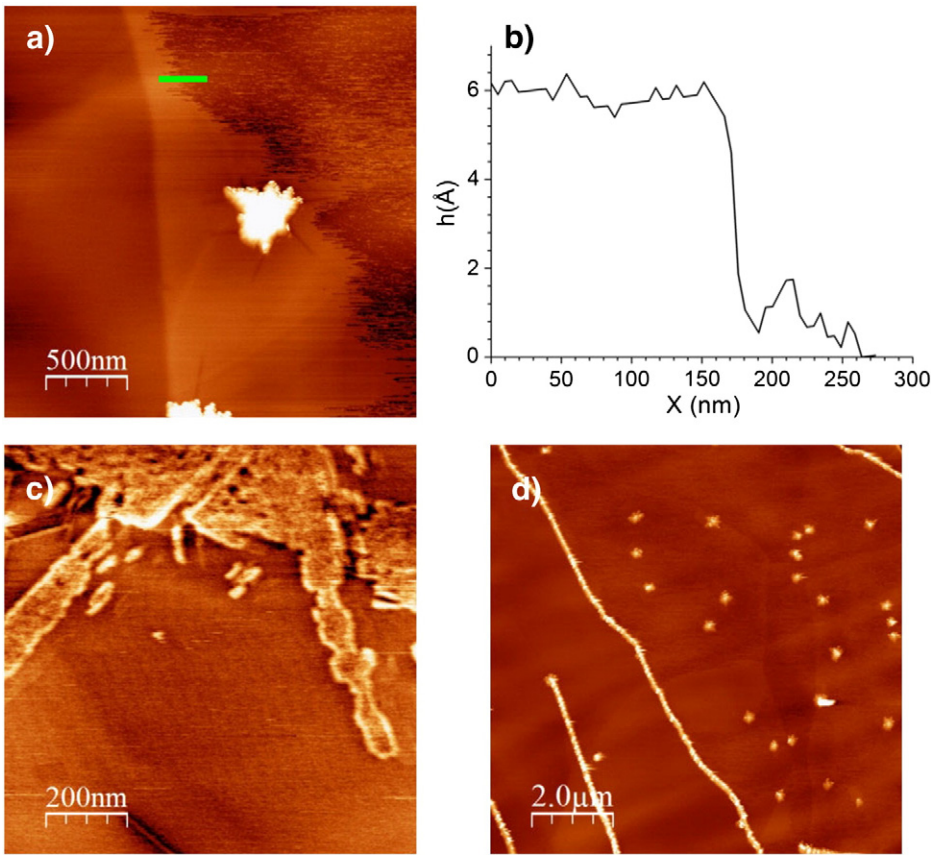

Fig. 6. a), c) and d) AFM images corresponding to 11 Eq-ML of CoO on HOPG where the wetting layer is clearly observable; b) topological profile of the wetting layer as indicated in a).

coverages up to around 30 Eq-ML (Fig. 1) whereas for the spectra of the SiO_2 substrate these species are dominant for coverages up to around 3 Eq-ML (Fig. 2). For very low coverages, a small part of metallic Cobalt (Co^0) remains unoxidized, giving rise to peak D in Figs. 1 and 2. For the HOPG substrate, metallic Co is observed up to ≈ 2 Eq-ML, whereas for the SiO_2 substrate they are visible only during the completion of the first Eq-ML. In regards to the significant presence of metallic Co for the early stages of growth of cobalt oxides on SiO_2, we want to point out that when CoO is grown on other different oxide substrates (MgO and Al_2O_3) CoO grows in a layer by layer mode [44] and no metallic Co is observed for the early stages of growth. One possible explanation for these results is the different coordinations of the Co atoms in CoO (octahedral) with respect to SiO_2 (tetrahedral), whereas the coordination of the other substrates (MgO and Al_2O_3) is the same as that of CoO.

The spectra for 80 Eq-ML on both substrates shows a 1 eV shift towards lower binding energies of the main peak and the appearance of the satellite peak B at 9–10 eV higher binding energy. This corresponds very well to the peaks in the calculated bottom spectrum of Fig. 3 and thus it is concluded that the spinel Co_3O_4 oxide is grown for the largest coverages on both surfaces. Similar results have also been found in the growth of Co oxides on different metallic substrates [22,45]. It is interesting to point out that although HOPG and SiO_2 exhibit very different surfaces, this does not affect the chemical state of the early stages of growth of the cobalt oxides, which is CoO in both cases. The same is true for the formation of the spinel Co_3O_4 oxide on the previous CoO deposits for large coverages on both substrates. However there is an important difference in the coverage at which the spinel oxide starts growing. The spectrum of Co_3O_4 is shifted by 1 eV towards lower binding energies with respect to that of CoO. In the case of the spectra of the HOPG substrate this shift is observable for coverages above 20 Eq-ML whereas for the SiO_2 substrate the shift is progressively produced at coverages above 3 Eq-ML. This suggests that Co_3O_4 starts growing at these coverages on the corresponding substrates. When the Co_3O_4 layer has grown up to a thickness larger than the inelastic mean free path of the Co 2p photoelectrons ($\lambda \approx 11$ Å for HOPG and $\lambda \approx 14$ Å for SiO_2 — this difference comes from the use of MgKα and AlKα radiation for excitation of the Co 2p electrons respectively), the spectra are dominated by the spectral shape of Co_3O_4 oxide, as in the case of the spectra corresponding to 80 Eq-ML on both substrates (Figs. 1 and 2).

3.2. Growth morphology: AFM versus XPS

3.2.1. CoO/HOPG

The AFM images taken for different coverages of the growth of Co oxides on HOPG are shown in Fig. 4. For the early stages of growth, CoO particles appear agglomerated at the steps of the HOPG surface, leading to the formation of structures along the steps of 100 Å heights. Once the steps have been completely filled in, dendritic structures start to grow and spread throughout the HOPG terraces, forming islands of variable height, ranging from 20 Å to 50 Å, for the early stages of growth, and from 70 Å to 80 Å for the intermediate stages. For coverages around 80 Eq-ML, full coverage of the substrate is observed.

In order to choose the most suitable model for the inelastic XPS peak shape analysis, the topography profile given in Fig. 5(a) shows that the CoO dendritic islands formed on both steps and terraces, have a sharp triangular profile, rather than a homogeneous height, with a maximum height of 120 Å. Accordingly, we have performed the inelastic XPS peak shape analysis using a linear distribution of island heights covering partially the substrate surface as depicted in the inset of Fig. 5(b). The results shown in Fig. 5b of island coverage versus maximum island height given by AFM and QUASES agree very well, showing e.g. that for coverages of 20 Eq-ML only 50% of the substrate surface is covered (the dashed curves in Fig. 5b correspond to constant Eq-ML curves). The results for the total Eq-ML coverage versus evaporation time show

a good agreement between AFM and QUASES results as shown in Fig. 5(c).

After a careful examination of the measured AFM images, the formation of a wetting layer is observed. The image of Fig. 6(a) shows a border separating two different regions with a step of approximately 4 Å, as depicted in the profile in Fig. 6(b). The lack of agglomerated islands on this border discards the possibility that this could be one of the HOPG steps. The height of the wetting layer given by the topographic profile agrees with the formation of one unit cell thick layer of CoO, which accounts for 2 ML in height. Similar images could easily be detected for samples with total coverage between 3 and 15 Eq-ML. Fig. 6(c) shows a detail of the wetting layer for a coverage of about 11 Eq-ML, where CoO domains grow following the three possible directions as dictated by the hexagonally arranged HOPG substrate. This preferential arrangement of the CoO atoms on the HOPG substrate shown in Fig. 6(c) suggests that CoO clusters autoassemble on the HOPG surface. Fig. 6(d) shows that CoO dendritic islands grow only on top of the CoO wetting layer.

By taking this information into account, a more complete model for the inelastic peak shape analysis consists of a model where a wetting layer of fixed thickness covers part of the surface and a fraction of this wetting layer is covered by planar islands as shown in the inset of Fig. 7a. Within this model the surface is divided into three regions: one fraction Cov_w is covered only with the wetting layer, another is covered with both the wetting layer and islands on top, and the third region is uncovered. By keeping the wetting layer height constant (4 Å) and subtracting the amount of material accumulated at the steps (determined in Fig. 5b) from the total deposited material, the fraction of the surface (Cov_w in the inset of Fig. 7a) which is covered only by the wetting layer, can be determined from analysis of the inelastic background. The results shown in Fig. 7a shows that Cov_w initially increases linearly with Eq-ML, goes through a maximum at ≈ 12–15 Eq-ML, and then drops off for larger deposits. This indicates that for 0–5 Eq-ML, the growth consists primarily in an increase of the extension of the wetting layer and in the range 5–12 Eq-ML, the islands start to grow on top of the wetting layer while the wetting layer is still expanding on the surface, at ≈ 15 Eq-ML the wetting layer covers the complete surface and for larger deposits, the islands continue to grow and cover ≈ 65% (=100–35% in Fig. 7a) of the surface at 20 Eq-ML. The total coverage as a function of the evaporation time is shown in Fig. 7(b). The results from the AFM data are also shown. The good agreement between the two techniques, gives confidence in the way of growth proposed.

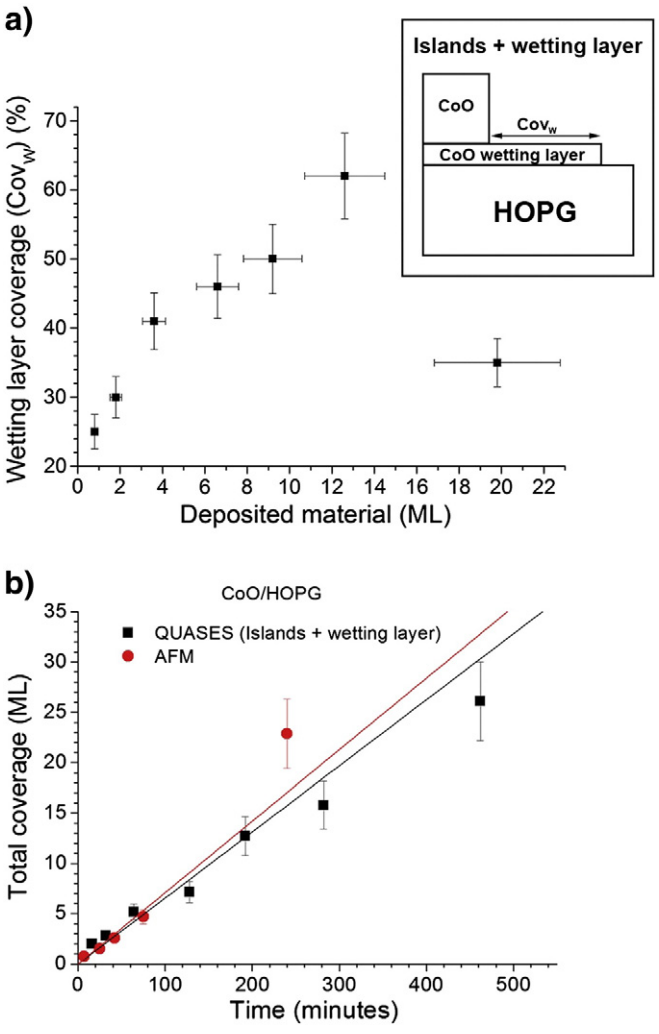

Fig. 7. a) Percentage of uncovered wetting layer as a function of deposited material given by inelastic XPS peak analysis; b) Comparison of the total amount of deposited material as a function of the growth time given by AFM (red dots) and inelastic XPS peak shape analysis (black squares).

According to the results shown above, we can conclude that, after the filling of the HOPG steps by small CoO nanoclusters, cobalt oxide grows following a Stranski–Krastanov growth mechanism with the formation of 2 CoO ML (1 unit cell) thick wetting layer followed by the growth of CoO islands on top. This kind of growth is typical for systems in which the adatom–surface interaction is larger than the adatom–adatom interaction. CoO deposits show a strong diffusion along the HOPG surface towards the steps, allowing the formation of an ultrathin CoO wetting layer by autoassembling.

3.2.2. CoO/SiO_2

The AFM images for different stages of growth of CoO on the SiO_2 substrate are shown in Fig. 8. The early stages of growth, as observed for coverages of 0.4 Eq-ML (Fig. 8a), consist of small CoO islands of about 8 Å in height which corresponds to the dimension of two CoO unit cells. A broad 10 × 10 μm^2 AFM image for this coverage is shown in Fig. 9. It is seen that bigger islands are formed by the aggregation of the smaller ones in the surrounding area, thus indicating a limited diffusion of the CoO adsorbates on the surface. The substrate appears almost fully covered at coverage of about 3 Eq-ML with islands whose height distribution ranges from 4 Å to 12 Å as shown in Fig. 8(b). While a first layer of islands is being formed, a second layer of islands of about 4 Å in height starts growing being this layer completed at coverages around 3 Eq-ML. Once this second layer has been completed, the images in Fig. 8(d) and (e) show that a flat thin film has been formed with no presence of islands on the surface. Even more, the mean roughness observed in the AFM images slightly decreases with increased coverages, reaching root mean square roughness (Rq) values in the range of those of the single crystal substrate.

According to the AFM images shown in Fig. 8, we have used a QUASES model which takes into account two sets of islands with different heights and coverages, as shown in the inset of Fig. 10(a). The results for the first and second island layers given by QUASES are seen to agree well with those from AFM (Fig. 10a), thus confirming the formation of a layer of islands of about 10 Å and a second layer of about 5 Å in height, and that this second layer is completed for 3 Eq-ML's. Finally, the good agreement between the two techniques is also shown in Fig. 10(b) from which it is seen that the total coverage as a function of the evaporation time, as deduced from AFM and QUASES, is identical to within ≈5%. Therefore, for the SiO_2 substrate the deposition of CoO follows a Volmer–Weber growth mode, with the formation of islands on the substrate. Once the island layer has been completed at coverages around 3 Eq-ML, a very flat thin film is formed with roughness of the same order as the initial single crystal SiO_2 substrate. We want to note that at this stage, the spinel Co_3O_4 oxide starts growing at the surface (see Section 3.1).

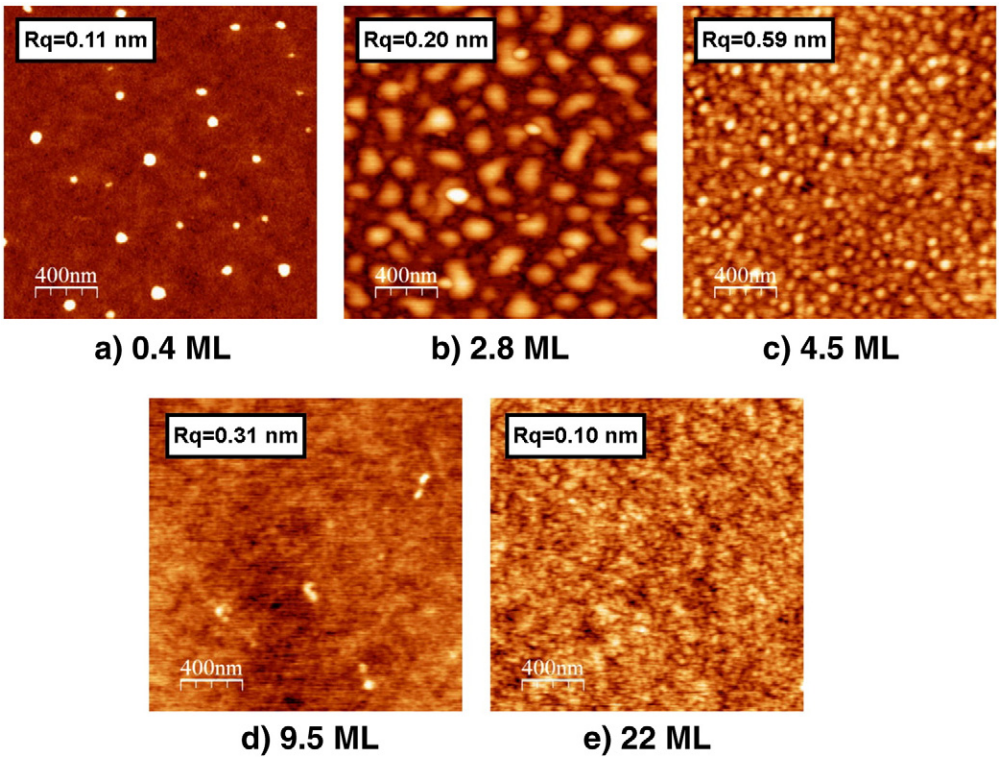

Fig. 8. $2 \times 2\ \mu m^2$ AFM images of the growth of Co oxides on SiO_2 for different coverages. The root mean square roughness (Rq) values are given.

The above results show that despite the very different surface structure and chemistry of the substrates studied here, the cobalt oxides grown on them have an identical chemistry i.e., the formation of CoO (Co^{2+}) oxide for the early stages of growth and the formation of the Co_3O_4 spinel structure for larger coverages. In contrast, the morphology and the way of the growth are completely different for the two substrates, being of the Stranski–Krastanov mode for HOPG and of Volmer–Weber mode for SiO_2. The key point to understand the different morphologies of the CoO deposits on both substrates is the strong diffusion observed on the HOPG substrate. This diffusion is probably due to the rapid oxidation of the metallic Co from the evaporator which reacts with oxygen, after dissociation of the oxygen molecule, forming CoO clusters. This conclusion is supported by Fig. 11 corresponding to the growth of 3 Eq-ML of metallic Co in ultra high vacuum conditions on a HOPG substrate at room temperature. The Co 2p XPS spectrum of this sample, shown in the inset of Fig. 11, is identical to that of metallic Co published elsewhere [46]. Fig. 11 shows that metallic Co grows on HOPG in a very different way to that of CoO observed in this work (see Figs. 4 and 8). The metallic Co deposits spread out on the HOPG surface as well as to the steps but they do not accumulate to the same extent as in the case of CoO showing limited surface diffusion. Therefore, the results suggest that the growth of CoO on HOPG is mainly characterized by strong diffusion of the CoO clusters across the graphite surface which leads to the formation of the autoassembled CoO wetting layer, whereas for the SiO_2 substrate the diffusion is limited to around 1 μm, as inferred from Fig. 9. In addition, the presence of unsaturated oxygen anions at the SiO_2 surface could be a reason for such a limited diffusion since the formation of M – O – Si (M = Ti, Ni) cross-linking bonds has been observed in the growth of TiO_2 [31,32] and NiO [30,33] oxides on SiO_2.

Regarding the chemical Co species formed on the two substrates during the growth process, two important questions arise. Firstly, how two very different surfaces give rise to the same chemical species and, secondly, why the same growth conditions lead to different Co species on both surfaces depending on the coverage i.e., Co^{2+} for low coverages and spinel ($Co^{2+,3+}$) for high coverages. One possible answer to the first question is that only these two Co oxides species are stable at room temperature and the growth conditions used in this work do not have enough oxidizing potential to oxidize cobalt directly to Co_3O_4, as is the case, for instance, for oxygen plasma used in Ref. [25]. In addition, at room temperature and equilibrium conditions, the reaction: $2\ Co + O_2 \rightarrow 2CoO$ is more probable than: $3\ Co + 2O_2 \rightarrow Co_3O_4$ [47]. In turn, the growth of the spinel Co_3O_4 on both substrates is observed for large deposition coverages, i.e., when coalescence has been produced with the formation of a continuous CoO overlayer. However, as discussed above, there are large differences in the coverage at which Co_3O_4 starts growing depending on the substrate. For HOPG, the structures formed at the early stages of growth are of the order of 140 Å in height (Fig. 5a and b) whereas those on the SiO_2 substrate are around 10 Å (Fig. 10a). As a consequence,

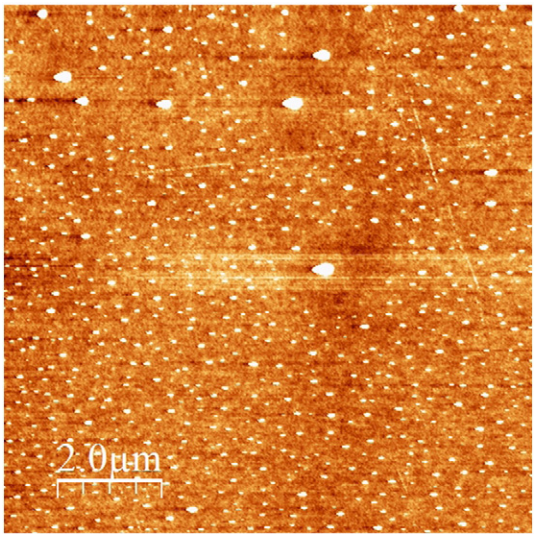

Fig. 9. $10 \times 10\ \mu m^2$ AFM image corresponding to 0.4 Eq-ML of CoO on SiO_2.

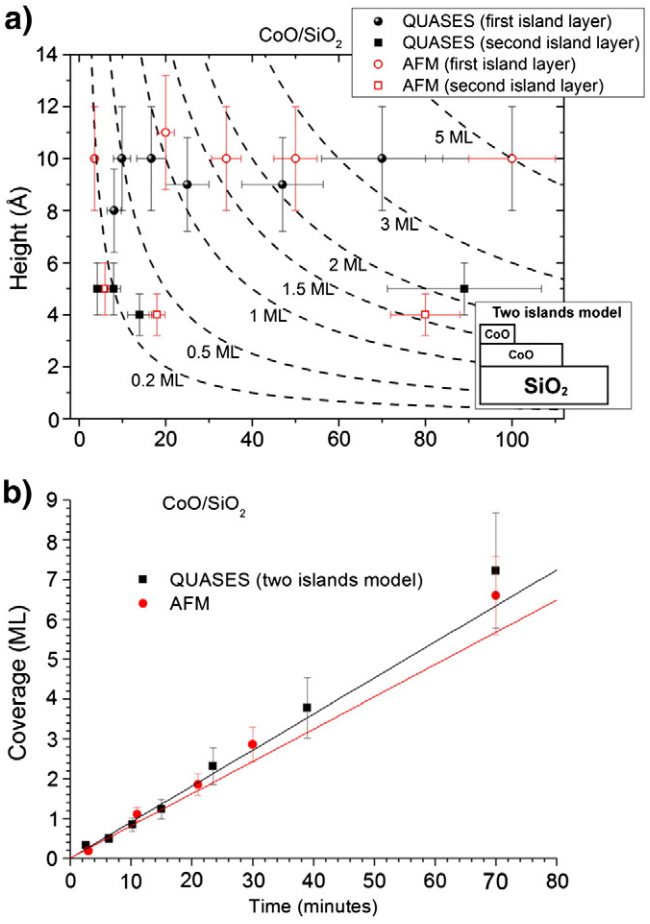

Fig. 10. a) Comparison of the quantitative information given by AFM (red symbols) and inelastic XPS peak shape analysis (black symbols) obtained by applying the two islands model; for the first (circles) and second island (squares) layers; b) Comparison of the total amount of deposited material as a function of the growth time given by AFM (red circles) and inelastic XPS peak shape analysis (black squares) using the two islands model.

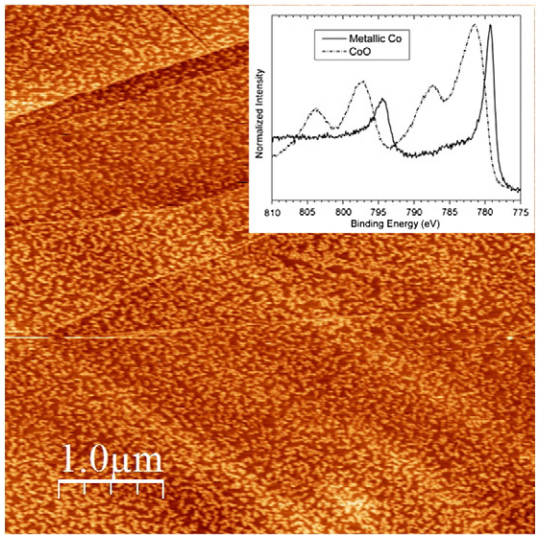

Fig. 11. 5 × 5 μm^2 AFM image of 3 Eq-ML of metallic Co grown on a HOPG substrate at room temperature in ultra-high vacuum conditions. The inset shows the Co 2p XPS spectrum of this sample compared to that of CoO.

coalescence is produced at different coverages, around 30 Eq-ML for HOPG (Fig. 5b) and around 5 Eq-ML for SiO_2 (Fig. 10a). These results are in complete agreement with those obtained from the Co 2p XPS spectra. They suggest that the surface energy of the CoO clusters is playing an important role. It is known that the surface energy of the CoO and Co_3O_4 nanoparticles strongly increases as the size of the nanoparticles decreases, and that this increase is much higher for CoO than for Co_3O_4 nanoparticles [48]. In this picture, when the topography of surface substrate does not present enough defects to allow the reduction of the surface energy of CoO, the spinel Co_3O_4 oxide starts to grow on the previously deposited CoO surface.

4. Conclusions

The early and final stages of the growth of cobalt oxide on HOPG and SiO_2 have been successfully studied both chemically and morphologically by XPS and AFM respectively, and we find good agreement between the results of these techniques. XPS chemical analysis reveals that, for both substrates, the early stages of growth are mainly formed by CoO (Co^{2+}) species, in contrast, further coverages lead to the formation of the spinel Co_3O_4 oxide ($Co^{2+,3+}$). This has been explained in terms of strong differences in the surface energy of CoO nanostructures grown on the two substrates. In the case of the HOPG substrate, the material grows following a Stranski–Krastanov growth mode, with the material first accumulating at the steps, and forming a unit cell thick wetting layer of CoO. Once this wetting layer has been formed, dendritic islands scattered across the terraces grow on it up to coverages of 30 Eq-ML. Strong diffusion of the CoO deposits along the HOPG surface has also been observed. This leads to the autoassembling of the CoO clusters following the directions dictated by the honeycomb surface structure of HOPG. For the SiO_2 substrate the material follows a Volmer–Weber growth mode, with the formation of a first layer of islands with a height of about 10 Å and a second layer of islands of about 4 Å in height. The CoO deposits are found to have much smaller surface diffusivity on SiO_2 than on to HOPG.

Acknowledgements

This investigation has been funded by the MINECO of Spain through the CONSOLIDER projects CSD2008-00023 and CSD2007-41 and projects ENE2010-21198-C04-04 and MAT2011-26534. One of the authors (O.B.M.) thanks the financial support from the “Ramón y Cajal” Program of MINECO.

References

[1] V.E. Henrich, Prog. Surf. Sci. 50 (1995) 77.
[2] V.E. Henrich, P.A. Cox, The Surface Science of Metal Oxides, Chap. 7, Cambridge University Press, Cambridge, 1994.
[3] R.J. Lad, Surf. Rev. Lett. 2 (1995) 109.
[4] S. Tougaard, J. Vac. Sci. Technol. A 8 (1990) 2197.
[5] S. Tougaard, QUASES. Software package for quantitative XPS/AES of surface nanostructures by inelastic peak shape analysis, see: www.QUASES.com.
[6] R. Kannan, M.S. Seehra, Phys. Rev. B 35 (1987) 6847.
[7] H. Landolt, R. Börnstein (Eds.), Landolt-Börnstein Zahlen-werteund Funktionenaus Naturwissenschaften und Technik: Neue Serie, Springer, Berlin, 1961.
[8] M. Hamdani, R.N. Singh, P. Chartier, Int. J. Electrochem. Sci. 5 (2010) 556.
[9] X.-C. Dong, H. Xu, X.-W. Wang, Y.-X. Huang, M.B. Chan-Park, H. Zhang, L.-H. Wang, W. Huang, P. Chen, ACS Nano 6 (2012) 3206.
[10] T.-Y. Wei, C.-H. Chen, K.-H. Chang, S.-Y. Lu, C.-C. Hu, Chem. Mater. 21 (2009) 3228.
[11] S. Yang, G. Cui, S. Pang, Q. Cao, U. Kolb, X. Feng, J. Maier, K. Mullen, ChemSusChem 3 (2010) 236.
[12] Z.-S. Wu, W. Ren, L. Wen, L. Gao, J. Zhao, Z. Chen, G. Zhou, F. Li, H.-M. Cheng, ACS Nano 4 (2010) 3187.
[13] F. Jiao, H. Frei, Angew. Chem. Int. Ed. 48 (2009) 1841.
[14] Y. Liang, Y. Li, H. Wang, J. Zhou, J. Wang, T. Regier, H. Dai, Nat. Mater. (2011) 10780.
[15] J. Park, X. Shen, G. Wang, Sens. Actuators, B Chem. 136 (2009) 494.
[16] J. Yang, W.-D. Zhang, S. Gunasekaran, Electrochem. Acta 56 (2011) 5538.
[17] H. Xing, W. Kong, C. Kim, S. Peng, S. Sun, Z. Xu, H. Zeng, J. Appl. Phys. 105 (2009) 063920.
[18] X.H. Xia, J.P. Tu, J. Zhang, J.Y. Xiang, X.L. Wang, X.B. Zhao, ACS Appl. Mater. Interfaces 2 (2010) 186.

[19] X.H. Xia, J.P. Tu, J. Zhang, J.Y. Xiang, X.L. Wang, X.B. Zhao, Sol. Energy Mater. Sol. Cells 94 (2010) 386.
[20] H.Y. Hwang, Y. Iwasa, M. Kawasaki, B. Keimer, N. Nagaosa, Y. Tokura, Nat. Mater. 11 (2012) 103.
[21] M. De Santis, A. Buchsbaum, P. Varga, M. Schmid, Phys. Rev. B 84 (2011) 125430.
[22] L. Gragnaniello, S. Agnoli, G. Parteder, A. Barolo, F. Bondino, F. Allegretti, S. Granozzi, G. Surnev, F. Netzer, Surf. Sci. 604 (2010) 2002.
[23] W. Meyer, K.M. Gubo, L. Hammer, K. Heinz, J. Phys. Condens. Matter 20 (2008) 265011.
[24] A.R. González-Elipe, F. Yubero, in: H.S. Nalwa (Ed.), Handbook of Surfaces and Interfaces of Materials, vol. 2, Academic Press, San Diego, 2001, (Chapter 4).
[25] V.M. Jiménez, J.P. Espinós, A.R. González-Elipe, Surf. Interface Anal. 26 (1998) 62.
[26] C.A.F. Vaz, D. Prabhakaran, E.I. Altman, V.E. Henrich, Phys. Rev. B 80 (2009) 155457.
[27] H. Sugimea, S. Nodaa, S. Maruyamab, Y. Yamaguchi, Carbon 47 (209) 234.
[28] A. Rizzetti, J. Xhie, K. Sattler, D. Yamamoto, W. Pong, J. Electron Spectrosc. Relat. Phenom. 58 (1992) 359.
[29] J. Xiao, S. Dunham, P. Liu, Y. Zhang, C. Kocabas, L. Moh, Y. Huang, K.-C. Hwang, Ch. Lu, W. Huang, J.A. Rogers, Nano Lett. 9 (2009) 4311.
[30] I. Preda, A. Gutiérrez, M. Abbate, F. Yubero, J. Méndez, L. Alvarez, L. Soriano, Phys. Rev. B 77 (2008) 075411.
[31] L. Soriano, G.G. Fuentes, C. Quirós, J.F. Trigo, J.M. Sanz, P.R. Bressler, A.R. González-Elipe, Langmuir 16 (2000) 7066.
[32] L. Soriano, M. Sánchez-Agudo, R.J.O. Mossanek, M. Abbate, G.G. Fuentes, P.R. Bressler, L. Alvarez, J. Méndez, A. Gutiérrez, J.M. Sanz, Surf. Sci. 605 (2011) 539.
[33] I. Preda, L. Soriano, D. Díaz-Fernández, G. Domínguez-Cañizares, A. Gutiérrez, G.R. Castro, J. Chaboy, J. Synchrotron Radiat. 20 (2013) 635.
[34] I. Horcas, R. Fernández, J.M. Gómez Rodríguez, J. Colchero, J. Gómez Herrero, A.M. Baró, Rev. Sci. Instrum. 78 (2007) 013705.
[35] G. van der Laan, C. Westra, C. Haas, G.A. Sawatzky, Phys. Rev. B 23 (1981) 4369.
[36] A. Fujimori, F. Minami, Phys. Rev. B 30 (1984) 957.
[37] J. van Elp, J.L. Wieland, H. Eskes, P. Kuiper, G.A. Sawatzky, Phys. Rev. B 44 (1991) 6090.
[38] M.P. Seah, in: D. Briggs, M.P. Seah (Eds.), 2nd ed., Practical Surface Analysis, vol. 1, John Wiley and Sons, Chichester, 1990, p. 245, (Chapter 5).
[39] R.W.G. Wyckoff, Crystal Structures II, Interscience, New York, 1964.
[40] S. Tougaard, Surf. Interface Anal. 26 (1998) 249.
[41] M.C. López-Santos, F. Yubero, J.P. Espinós, A.R. González-Elipe, Anal. Bioanal. Chem. 396 (2010) 2757.
[42] I. Preda, L. Soriano, L. Alvarez, J. Méndez, F. Yubero, A. Gutiérrez, J.M. Sanz, Surf. Interface Anal. 42 (2010) 869.
[43] National Institute of Standards and Technology; X-ray Photoelectron Spectroscopy (XPS) Database, 2013.
[44] D. Díaz-Fernández, J. Méndez, F. Yubero, G. Domínguez-Cañizares, A. Gutiérrez, L. Soriano, Surface and Interface Analysis 16 (2014) http://dx.doi.org/10.1002/sia.5366.
[45] W. Meyer, K. Biedermann, M. Gubo, L. Hammer, K. Heinz, J. Phys. Condens. Matter 20 (2008) 265011.
[46] M.C. Biesinger, B.P. Payne, A.P. Grosvenor, L.W.M. Lau, A.R. Gerson, R.St.C. Smart, Appl. Surf. Sci. 257 (2011) 2717.
[47] H.J.T. Ellingham, J. Soc. Chem. Ind. 63 (1944) 125.
[48] A. Navrotsky, Ch. Ma, K. Lilova, N. Birkner, Science 30 (2010) 199.